Thermodynamic and transport coefficients from the dynamic structure factor of Yukawa liquids

Hanno Kählert
Christian-Albrechts-Universität zu Kiel, Institut für Theoretische Physik und Astrophysik, Leibnizstr. 15, 24098 Kiel, Germany

(Received 26 April 2020; accepted 6 August 2020; published 21 August 2020)

The ion-ion dynamic structure factor (DSF) of warm dense matter and dense plasmas contains information on collective ionic modes and various thermodynamic and transport coefficients, which are important for modeling the interiors of giant planets or the dense plasmas occurring in inertial confinement fusion. Here, it is demonstrated, using the Yukawa liquid as a reduced model, that the complete hydrodynamic information encoded in the DSF can be extracted with an accuracy comparable to that of dedicated methods. This is achieved by applying a generalized hydrodynamic and a viscoelastic model and extrapolating the results at finite wave numbers into the hydrodynamic limit. Very good agreement with previous data is obtained for the sound speed and the viscosity. The thermal diffusivities deduced from different methods exhibit somewhat larger deviations.

DOI: 10.1103/PhysRevResearch.2.033287

I. INTRODUCTION

Warm dense matter (WDM) is an unusual state of matter—between a solid and a fully ionized plasma—with solid densities, megabar pressures, and temperatures in the eV range [1]. At keV temperatures, one enters the regime of a hot dense plasma [2]. Matter at such extreme conditions is characterized by partial ionization, moderately coupled and partially degenerate electrons, and strongly coupled classical ions. The thermodynamic and transport properties of WDM and dense plasmas are of high importance for a variety of fields, including planetary science [3–5] and astrophysics [6,7], and for the advancement of inertial confinement fusion concepts [8–10].

Various methods have been devised for the creation and diagnostic of these exotic states [11]. In particular, x-ray scattering provides detailed insights into their properties [12–17]. The analysis of collective modes of the electrons [18], e.g., gives access to the electron density and temperature [19,20], and the electrical conductivity [21]. A significant step forward can be expected from the LCLS at Stanford [22] or the European XFEL [23]. In particular, it should become possible to diagnose collective modes of the *ions* [24], which carry information on fundamental material properties such as the viscosity but are very difficult to resolve. Within the Chihara decomposition [25] of the total electron dynamic structure factor, which determines the scattering signal [13], they manifest themselves in the ion-ion dynamic structure factor (DSF).

In recent years, significant efforts have been made to compute the ion-ion DSF from *ab initio* simulations [26], combining a classical description of the ions with a quantum treatment of the electrons [27–31]. The computational cost can be reduced by employing effective ion-ion pair potentials [32–34]. Several theoretical models have been proposed to describe the DSF in dense plasmas and WDM. Mithen *et al.* [35] have used the hydrodynamic result to model the DSF of a strongly coupled Yukawa liquid and later extended their investigations via the memory function formalism [36,37]. Vorberger *et al.* [38] performed a comparison of various models [35,39–41] for the DSF of shocked Silicon, computed from simulations with a modified Yukawa potential. Recently, Choi *et al.* [42] performed a similar comparison for Coulomb and Yukawa liquids. Arkhipov *et al.* [43] used the moments method to investigate the DSF of Coulomb and Yukawa one-component plasmas.

Rather than attempting to reproduce the DSF with as few free parameters as possible, a different goal is pursued in this work. In the hydrodynamic limit, the DSF contains information on the fundamental thermodynamic and transport properties of a liquid [44–46]. Here, it is demonstrated that this can be exploited to extract various hydrodynamic properties of strongly coupled Yukawa liquids solely from the DSF. The Yukawa model is chosen for two reasons. First, it has been used as a simplified model for a reduced description of WDM and dense plasmas [2,34,47]. For a direct comparison with experimental or *ab initio* simulation data, a short-ranged repulsive potential can be added to the Yukawa potential to capture effects related to bound electrons and to better match the ion structural properties [20,38,48]. Second, and more importantly, a large amount of accurate data are available for the thermodynamic [49–51] and transport properties [52–56], which will be used to demonstrate the feasibility of the method. The methodology could provide a practical means for the determination of hydrodynamic coefficients (e.g., viscosity) from experimental and simulation data for the ion-ion DSF of WDM and dense plasmas, which are of high importance for simulations of inertial confinement fusion implosions or the modeling of planetary interiors. Since the Yukawa liquid is a very general model system, the results could also be relevant to ultracold neutral plasmas [57], dusty

(complex) plasmas [58], or colloidal dispersions [59]. In the latter two cases, however, frictional damping is important.

The analysis of Mithen *et al.* [35] has shown that the Rayleigh-Brillouin triplet [44,46] accurately describes the DSF of Yukawa liquids at small wave numbers k. It consists of a central Lorentzian line, representing a diffusive heat mode, and two shifted Lorentzians, representing propagating sound modes. The hydrodynamic parameters determine their widths and intensities. When fitted to the DSF at a single wave number [35,37], the model gave hydrodynamics coefficients that were in reasonable agreement with the available data at the time. In this work, the DSF is analyzed using two extensions of the hydrodynamic model. In the generalized hydrodynamic (GH) model [60], the frequency dependence of the hydrodynamic DSF is left unchanged but the peak intensities and widths can have an arbitrary k dependence. The viscoelastic (VE) model extends hydrodynamics to finite frequencies by introducing the concept of viscoelasticity. Here, the DSF contains an additional central Lorentzian peak, which vanishes in the hydrodynamic limit [60]. By (i) fitting the model parameters to simulation data and (ii) extrapolating the results to $k \to 0$ (similar to recent work by Guarini *et al.* [61] and Silvestri *et al.* [62]), the complete thermodynamic and transport properties contained in the DSF are obtained, with an accuracy comparable to dedicated other methods [52–56]. The VE model allows one to go beyond a purely hydrodynamic description and yields results for the viscoelastic properties.

This paper is organized as follows. A brief description of the simulation method is given in Sec. II. The two models used for the DSF and their relation to the hydrodynamic limit are introduced in Sec. III. Results for the DSF and the hydrodynamic parameters are presented and discussed in Sec. IV. Section V provides a brief summary and outlook.

II. SIMULATIONS

Molecular dynamics (MD) simulations are carried out for particles of mass m interacting via the Yukawa potential, $v(r) = q^2 \exp(-r/\lambda_s)/r$, where q is the particle charge and λ_s the screening length. The screening parameter, $\kappa = a/\lambda_s$, where $a = (3/4\pi n)^{1/3}$ is the Wigner-Seitz radius and n the particle density, is chosen as $\kappa = 2$. The reason is that a large body of data for the transport coefficients are available [52–56]. The values for the coupling parameter, $\Gamma = q^2/(a\, k_B T)$, where T is the temperature, are in the range $\Gamma = 10, \ldots, 200$, covering a wide range of conditions – from a moderately coupled system at $\Gamma/\Gamma_m \approx 0.02$ up to a strongly coupled liquid at $\Gamma/\Gamma_m \approx 0.5$, where $\Gamma_m \approx 440$ is the melting point [49]. Two sets of simulations were carried out using $N = 3800$ and $N = 5000$ particles, which gives access to wave numbers with $ka \gtrsim 0.23$.[1] The dynamic structure factor, which is defined in terms of the intermediate scattering function, $F(k,t) = N^{-1}\langle n_{\boldsymbol{k}}(t) n_{-\boldsymbol{k}}(0)\rangle$, as

$$S(k,\omega) = \frac{1}{2\pi}\int_{-\infty}^{\infty} F(k,t) e^{i\omega t}\, dt, \tag{1}$$

is computed from the Fourier transform of $n_{\boldsymbol{k}}(t) = \sum_{i=1}^{N} e^{-i\boldsymbol{k}\cdot\boldsymbol{r}_i(t)}$ [63].

[1] Data for $N = 3800$ at $\Gamma = 10$ and $\Gamma = 200$ from Ref. [63] are used again for the present analysis.

III. THEORY

As discussed above, the hydrodynamic result for the DSF can be written as the sum of a central Lorentzian (will be referred to as "heat mode") and two shifted Lorentzians ("sound modes") [44,46]. Compared to some of the previous applications in the field of WDM [32,35,38,64], the asymmetry of the latter [45] is taken into account, which leads to a finite second frequency moment [60]. Following Bafile *et al.* [60], the generalized hydrodynamics (GH) model is written as

$$\frac{\pi\, S^{\mathrm{GH}}(k,\omega)}{S(k)} = \frac{I_h\, z_h}{\omega^2 + z_h^2} + I_s \sum_{m=\pm 1} \frac{z_s + m\, b_s(\omega + m\,\omega_s)}{(\omega + m\,\omega_s)^2 + z_s^2}, \tag{2}$$

where $S(k)$ is the static structure factor, I_h [$I_s = (1 - I_h)/2$] denotes the intensity of the heat (sound) peak and z_h (z_s) its width. The parameter $b_s = \omega_s^{-1}[z_s + z_h I_h/(1 - I_h)]$ describes the asymmetry of the sound peaks. In the hydrodynamic limit, the parameters are given by, to lowest order in k, $z_h = D_T k^2$, $z_s = \Gamma_s k^2 = [(\gamma - 1)D_T + \nu_l]k^2/2$, $I_h = 1 - \gamma^{-1}$, and $\omega_s = c_s k$. Here, D_T is the thermal diffusivity, Γ_s the sound attenuation coefficient, $\gamma = c_p/c_v$ the adiabatic index (with specific heats at constant pressure and volume, c_p and c_v, respectively), $\nu_l = (4\,\eta_s/3 + \eta_b)/(nm)$ the longitudinal kinematic viscosity (with the shear viscosity η_s and the bulk viscosity η_b), and c_s the adiabatic sound speed [45,60].

The VE model is typically formulated in the framework of the memory function formalism [44–46], where the instantaneous decay of the viscous term in the hydrodynamic model is replaced by an exponential decay [60]. It has been shown [60] that it can be expressed, at small k, in the same form as the GH model but with an additional central Lorentzian (intensity I_2, width z_2),

$$\frac{\pi\, S^{\mathrm{VE}}(k,\omega)}{S(k)} = \frac{I_h\, z_h}{\omega^2 + z_h^2} + \frac{I_2\, z_2}{\omega^2 + z_2^2} + I_s \sum_{m=\pm 1} \frac{z_s + m\, b_s(\omega + m\,\omega_s)}{(\omega + m\,\omega_s)^2 + z_s^2}, \tag{3}$$

where now $b_s = \omega_s^{-1}[z_s + (I_h z_h + I_2 z_2)/(1 - I_h - I_2)]$ and $I_s = (1 - I_h - I_2)/2$. The intensity I_2 can be written in terms of z_h, z_s, z_2, ω_s, and I_h as

$$I_2 = \frac{z_s^2 + \omega_s^2}{(z_2 - z_s)^2 + \omega_s^2} \frac{z_h}{z_h - z_2}\left[1 - \alpha\, \frac{z_2(2\,z_s + z_h)}{z_h(2\,z_s + z_2)}\right], \tag{4}$$

$$\alpha = 1 - I_h \frac{(z_h - z_s)^2 + \omega_s^2}{z_s^2 + \omega_s^2}\left(\frac{z_2 - z_h}{z_2}\right). \tag{5}$$

In the limit $k \to 0$, I_2 should vanish as $I_2 \propto k^4$ while the width z_2 should turn into a constant, $z_2 \to 1/\tau$, to be consistent with the hydrodynamic limit. Here, τ is the $k \to 0$ limit of the viscoelastic relaxation time. Theory shows that for consistency with hydrodynamics, τ is given by $\tau = \nu_l/(c_L^2 - c_s^2)$, where c_L is the $k = 0$ limit of the infinite-frequency (longitudinal) sound speed [60]. A liquid shows elastic response for frequencies $\omega \gg \tau^{-1}$ while viscous behavior is found at low

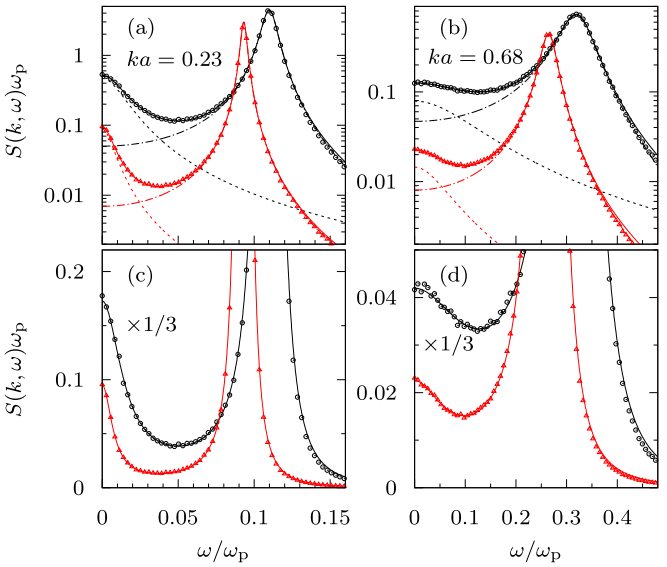

FIG. 1. Comparison of the GH fit with the MD data for $\Gamma = 10$ (black, circles) and $\Gamma = 50$ (red, triangles). The wave number is $ka = 0.23$ in (a) and (c) and $ka = 0.68$ in (b) and (d). The contribution of the heat (sound) mode is shown by the dashed (dashed-dotted) line. For a better presentation, the data for $\Gamma = 10$ in (c) and (d) have been multiplied by a factor 1/3.

frequencies, $\omega \ll \tau^{-1}$. The widths and intensities of the heat and sound peak have the same limits as above. Compared to the GH model, the VE model has a finite fourth moment [60]. Both models can be considered few-term approximations of an exact expansion of the DSF in a series of Lorentzian functions [65]. The parameters of the memory function can be reconstructed from the above parameters, if necessary. In particular, Bafile *et al.* [60] provide explicit formulas for $\omega_k^2(k) = \langle\omega^2\rangle/S(k)$ and $\omega_L^2(k) = \langle\omega^4\rangle/\langle\omega^2\rangle$ (only VE), where $\langle\omega^k\rangle$ are the frequency moments of the DSF.

A least-squares fit is used to determine the widths z_h, z_s, z_2, the frequency of the sound mode, ω_s, and the intensity I_h. In addition, the static structure factor is used as a fit parameter. All other parameters follow from the model. Since the DSF decays very rapidly at high frequencies [42,66], the fit region for Eq. (2) is restricted to the central peak and the main body of the sound peak [$\omega \lesssim \omega_s(k) + z_s(k)$]. The VE model is applicable at higher frequencies, and a larger fit range has been chosen, $\omega < 0.4\,\omega_p$, where $\omega_p = \sqrt{4\pi q^2 n/m}$ is the plasma frequency.

IV. RESULTS

A. Dynamic structure factor

A comparison between the simulation data and the GH fit is shown in Fig. 1.[2] While the model provides a very good fit function for the low-frequency part, the DSF decays faster at high frequencies. Also shown are the individual contributions of the heat and sound peaks from Eq. (2). At $ka = 0.23$, the central peak is almost fully reproduced by the heat mode while at $ka = 0.68$ the sound mode makes an important contribution at $\omega = 0$. A similar comparison is shown in Fig. 2 for the VE model. One observes that the VE model accurately describes the decay of the DSF immediately following the sound peak. Figure 2(d) shows the intensities of the various peaks. The intensity of the second central peak, I_2, is consistent with a k^4 decay in the $k \to 0$ limit, as anticipated from theoretical considerations [60] and discussed above.

B. Fit parameters and extrapolation

The fit parameters are shown in Fig. 3. Their $k \to 0$ limits yield values for (a) the sound speed, (c) the sound attenuation coefficient, (d) the inverse of the viscoelastic relaxation time, and (e) the thermal diffusivity. Figure 3(b) shows $I_h/(2I_s)$, which reduces to the Landau-Placzek ratio, $I_h/(2I_s) \to \gamma - 1$, in the hydrodynamic limit [46]. The hydrodynamic scaling, $\omega_s \to c_s k$, $z_s \to \Gamma_s k^2$, and $z_h \to D_T k^2$, has been removed. For the isotropic liquid, a simple polynomial ansatz with even powers of $\bar{k} = ka$, $f(\bar{k}) = c_0 + c_2\bar{k}^2 + c_4\bar{k}^4$, is used for the estimation of the hydrodynamic coefficient, c_0. In some cases, a simple average over the first few values has been employed instead. In particular for intermediate coupling strengths, $30 \lesssim \Gamma \lesssim 70$, the hydrodynamic scaling is excellent, and the remaining dependence on k is typically weak, see

[2]Note that the number of data points has been reduced for a better presentation.

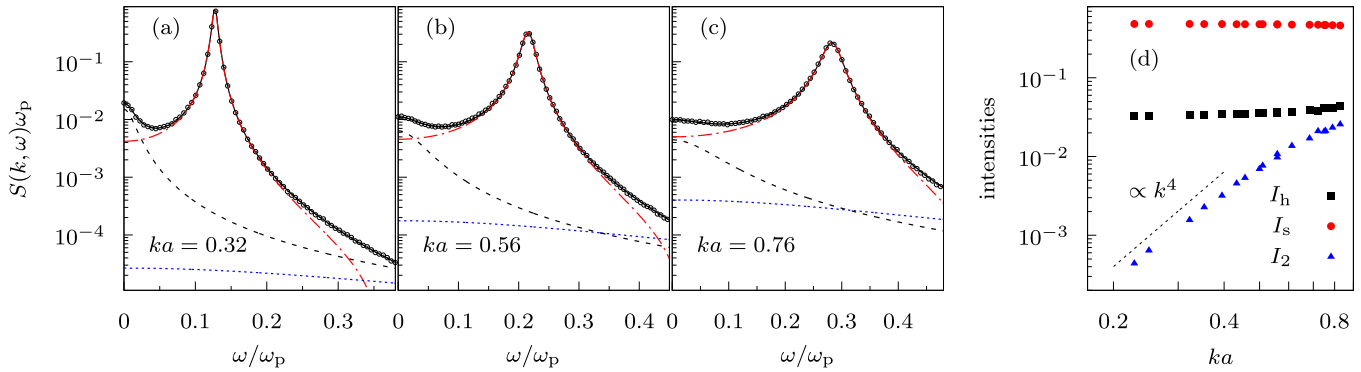

FIG. 2. [(a)–(c)] Comparison of the VE model (full line) with the MD data (circles) for $\Gamma = 100$. Also shown are the contributions of the heat mode (dashed line), the sound mode (dashed-dotted), and the second central line (dotted). (d) shows their respective intensities. The dashed line indicates a $\propto k^4$ behavior.

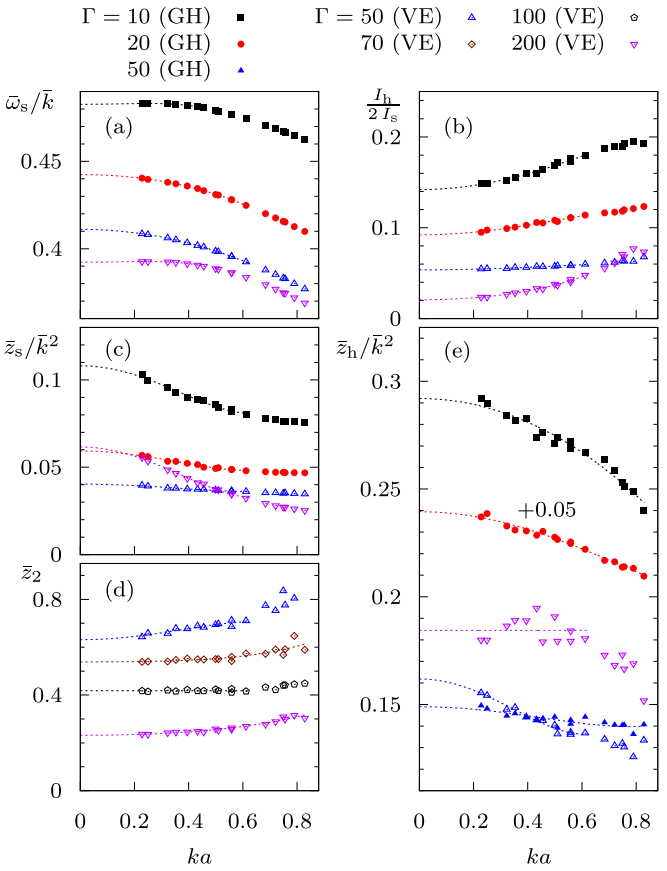

FIG. 3. Fit parameters obtained from the GH and VE model. The parameters in (a), (c), and (e) have been scaled by inverse powers of $\bar{k} = ka$ such that they reduce to constant values (the hydrodynamic coefficients) in the $\bar{k} \to 0$ limit. All frequencies are given in units of the plasma frequency, denoted by a bar. Dashed lines show the fits used for the extrapolation. They are shown in their respective fit range. Data in (e) for $\Gamma = 20$ have been shifted for clarity.

$\Gamma = 50$. The thermal diffusivity is the most difficult quantity to determine (e.g., $\Gamma = 10$ and 200), which is possibly related to the smallness of the central peak, in particular at strong coupling. Interestingly, the sound dispersion, $\omega_s(k)$, appears to change from negative to positive for $\Gamma \lesssim 10$ and $\Gamma \gtrsim 200$. However, larger simulations would be required to confirm this behavior.

C. Thermodynamic and transport data

The thermodynamic coefficients obtained from the extrapolation are shown in Fig. 4. For comparison, recent data for the sound speed by Silvestri *et al.* [62] and data obtained from fits for the internal energy of a single-component Yukawa fluid (without background terms) from Khrapak and Thomas [50,51] are included. Note that the sound speed and the adiabatic index are related by $c_s^2 = \gamma/(n\,m\,\chi_T)$, where χ_T is the isothermal compressibility [44,46]. Excellent agreement is found between all data sets for the sound speed (deviations $\lesssim 1\%$). The adiabatic index from the present analysis is slightly smaller than the analytical result for $\Gamma \lesssim 20$. For larger Γ, the agreement is very good.

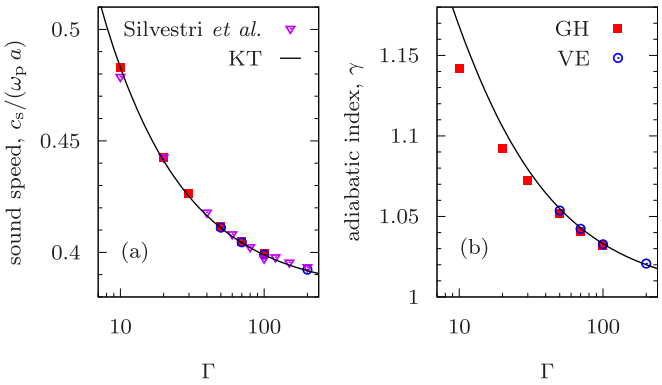

FIG. 4. (a) Sound speed and (b) adiabatic index as obtained from the GH and VE models. The sound speed and adiabatic index obtained from the internal energy of Khrapak and Thomas (KT) [50,51] and the MD results of Silvestri *et al.* [62] are shown for comparison.

Figure 5 depicts the results for the transport coefficients. Recent data for the thermal diffusivity D_T are available from the work of Ott *et al.* [56]. In addition, D_T can be computed from the thermal conductivity λ and c_p via $D_T = \lambda/(n\,c_p)$ [45,60]. While results for λ are available from Refs. [52,55], c_p is calculated from the fits of Refs. [50,51]. The results for D_T obtained in the present work are in very good agreement with the corresponding values of Ott *et al.* (OBHD) [56], albeit slightly lower ($\approx$5%–10%). Good agreement is also observed when the nonequilibrium results for λ of Donkó and Hartmann [52] are used (DH-KT). The Green-Kubo data of Ott *et al.* (OBD-KT) [55] yield somewhat larger values (roughly 10%−20%, 25% larger than GH at $\Gamma = 70$), as noted previously [56]. The longitudinal viscosity, $\nu_l = 2\,\Gamma_s - (\gamma - 1)D_T$, is shown in Fig. 5(b). The mutual agreement between data in the literature [53,54] and the present results is very good, with particularly small deviations in the range $\Gamma \approx 30, \ldots, 100$. The GH and VE model yield almost identical results and even allow one to determine the famous viscosity minimum. The interpolation formula of Khrapak [67] provides an accurate analytical expression for the viscosity.

D. Relaxation time and infinite-frequency sound speeds

Figure 3(d) shows that the inverse relaxation time, $\tau^{-1} = \lim_{k\to 0} z_2(k)$, decreases with the coupling strength, i.e., the transition from viscous to elastic response takes place at increasingly lower frequencies. Using the previous data for ν_L, c_s, and τ in the relation $\tau = \nu_l/(c_L^2 - c_s^2)$ (see Sec. III), one may compute a value for c_L, which can be compared with the theoretical value. The latter is related to the high-frequency shear (G_∞) and bulk (K_∞) elastic moduli and the $k \to 0$ limit of $\omega_L^2(k) = \langle\omega^4\rangle/\langle\omega^2\rangle$ [45,60],

$$c_L^2 = \frac{1}{m\,n}\left(\frac{4}{3}G_\infty + K_\infty\right) = \lim_{k\to 0}\frac{\omega_L^2(k)}{k^2}. \qquad (6)$$

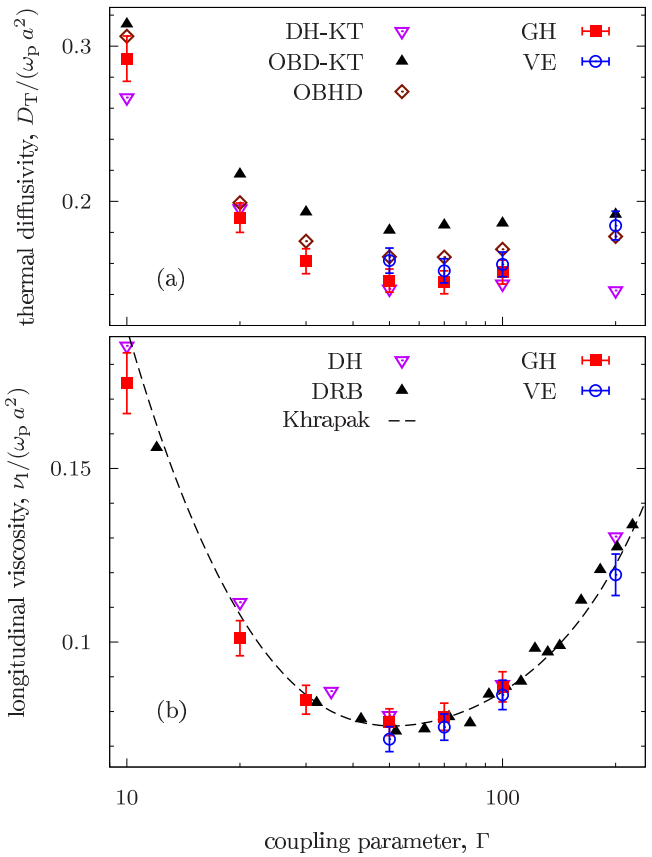

FIG. 5. (a) Thermal diffusivity and (b) longitudinal viscosity from the GH and VE models, shown with 5% error bars for a better assessment of the deviations. Results for the thermal conductivity of Donkó and Hartmann (DH-KT) [52] and Ott, Bonitz, and Donkó (OBD-KT) [55] have been used to calculate D_T via $D_T = \lambda/(n\,c_p)$, see the text for details. Also shown are the results for D_T from Ref. [56] (OBHD). The shear viscosities of Donkó and Hartmann (DH) [53] and Daligault, Rasmussen and Baalrud (DRB) [54], and the interpolation formula of Khrapak [67] have been used to compute the longitudinal viscosity from $\nu_l \approx 4\,\eta_s/(3\,n\,m)$. The bulk viscosity is negligible [68] and has been neglected.

The elastic moduli have been calculated as specific integrals over the pair distribution function involving derivatives of the Yukawa potential [45,69],

$$G_\infty = nk_BT + \frac{2\pi\,n^2}{15}\int_0^\infty g(r)\frac{d}{dr}[v'(r)r^4]dr, \tag{7}$$

$$K_\infty = \frac{5}{3}G_\infty + 2(p - nk_BT), \tag{8}$$

$$p = nk_BT - \frac{2\pi\,n^2}{3}\int_0^\infty g(r)v'(r)r^3dr. \tag{9}$$

Here, p is the pressure and $g(r)$ the pair distribution function.

The results are shown in Fig. 6. Figure 6(a) shows that the calculation of c_L from the extrapolation of the various fit parameters is consistent with the $k \to 0$ limit of $\omega_L(k)/k$, using the provided formula in Ref. [60]. The same applies to the data taken directly from the moments of the DSF

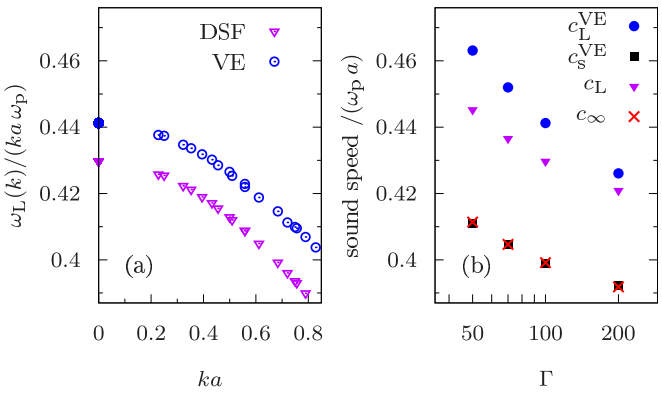

FIG. 6. (a) The ratio $\omega_L(k)/k$ as obtained from the moments of the DSF and the VE fit (see text) for $\Gamma = 100$. The filled symbols at $k = 0$ show a calculation of c_L via the elastic moduli [Eq. (6), triangle] and from the relation $c_L^2 = c_s^2 + \nu_L/\tau$ with the extrapolated fit parameters (circle). These values are shown in (b) as a function of the coupling strength. Also depicted are the adiabatic sound speed c_s from the VE model and the infinite-frequency sound speed c_∞.

and the calculation of c_L via the pair distribution function. However, there is a shift between these data, mainly caused by an overestimation of the fourth moment in the VE model.[3] This could be related to the very fast decay of the DSF in the high-frequency limit (see also Ref. [42]), which becomes increasingly important for the high-order moments. The resulting deviations for c_L are on the order of a few percent and decrease with the coupling strength, see Fig. 6(b). Even though the deviations from the theoretical value are rather

[3]Similarly, the GH model overestimates the second moment.

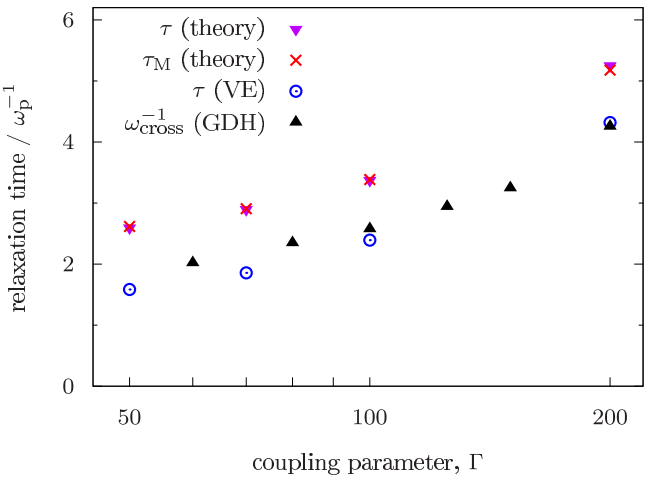

FIG. 7. Relaxation times as a function of Γ. Shown are calculations of τ and τ_M via Eq. (10) (theory), where the shear viscosity has been taken from the interpolation formula of Khrapak [67] (bulk viscosity neglected for τ) and the VE value for c_s has been used. Elastic moduli have been calculated via the pair distribution function. Also shown are the VE value for τ from the extrapolation and the inverse crossover frequency of the complex shear viscosity computed by Goree, Donkó, and Hartmann (GDH) [72].

TABLE I. Adiabatic sound speed, thermal diffusivity, and longitudinal viscosity from the GH and VE models ($\kappa = 2$).

	$c_s/(\omega_p\, a)$		$D_T/(\omega_p\, a^2)$		$\nu_L/(\omega_p\, a^2)$	
Γ	GH	VE	GH	VE	GH	VE
10	0.483		0.292		0.175	
20	0.442		0.189		0.101	
30	0.426		0.161		0.0834	
50	0.412	0.411	0.149	0.162	0.0769	0.0720
70	0.405	0.404	0.148	0.155	0.0785	0.0755
100	0.399	0.399	0.154	0.159	0.0871	0.0848
200		0.392		0.184		0.119

small, they can significantly affect τ as c_L and c_s are of the same order [see Fig. 6(b)] and $\tau \propto (c_L^2 - c_s^2)^{-1}$, see the discussion below.

A related quantity is the infinite-frequency sound speed $c_\infty = \sqrt{K_\infty/(mn)}$ [70,71], which involves the (high-frequency) bulk modulus only. Note that in the present case, the kinetic terms $\sim nk_BT$ are included in the calculation of the elastic moduli. As shown in Fig. 6(b), c_∞ is in excellent agreement with the adiabatic sound speed c_s, in line with previous results for Yukawa [70] and soft inverse power-law interactions [71]. Using the approximations $c_s \approx c_\infty$ and $\nu_l \approx 4\,\eta_s/(3nm)$ (neglecting the bulk viscosity), and making use of the relation $c_L^2 = c_\infty^2 + 4\,G_\infty/(3\,nm)$, one obtains, for the theoretical value of the relaxation time,

$$\tau = \frac{\nu_l}{c_L^2 - c_s^2} \approx \frac{\eta_s}{G_\infty} = \tau_M. \tag{10}$$

Here, τ_M is the Maxwell relaxation time [45,72], which describes shear relaxation in a liquid. As shown in Fig. 7, the theoretical value for τ practically coincides with τ_M. As could be anticipated from the discussion above, the VE value for τ is somewhat lower, in particular at intermediate coupling strengths. On the other hand, it is in rather good agreement with the inverse crossover frequency of the real and complex parts of the generalized *shear viscosity* determined by Goree *et al.* [72], which was used as an empirical measure of τ_M. A more detailed investigation of these aspects would be required but is beyond the scope of this work.

E. Discussion

In summary, the analysis of the DSF at small frequencies and wave numbers can yield comprehensive insights into the hydrodynamic properties of Yukawa liquids. Compared to other approaches such as nonequilibrium or Green-Kubo methods, which typically only yield one particular transport coefficient, the method used here allows one to estimate several coefficients at the same time. On the other hand, it relies (i) on a specific model for the DSF and (ii) an extrapolation scheme, which must be sufficiently accurate to avoid systematic errors. Comparisons with a variety of available data sets show that the deviations from the results of other methods are relatively small, in particular for the sound speed ($\lesssim 1\%$) and the viscosity ($\sim 5\%$–10%). The largest deviations among different methods are found for the thermal diffusivity, which requires further investigation. For reference, the adiabatic sound speed and the transport coefficients are summarized in Table I.

V. CONCLUSION

It has been demonstrated that fundamental thermodynamic and transport properties of Yukawa liquids can be obtained with high accuracy from an analysis of the DSF. The VE model even allows one to quantify viscoelasticity in the strongly coupled liquid regime, giving access to properties beyond a purely hydrodynamic description. It remains to test the applicability of the method for a wider range of screening and coupling parameters. The analysis of Mithen *et al.* [35] suggests that it could be easier to apply the method at stronger screening, where the applicability range of the hydrodynamic model becomes larger. On the other hand, in the very weakly coupled limit, it has recently been shown [62] that the acoustic peak disappears below a critical Γ, rendering the applicability of the hydrodynamic approach doubtful in this regime. Note that other extensions of hydrodynamics to finite ω and k (see, e.g., Refs. [36,60]) could be more appropriate than the GH or VE model under certain conditions.

For *ab initio* (density functional theory based) MD simulations in the WDM regime, it may become difficult to reach sufficiently small wave numbers since the number of particles that can be simulated is much smaller than for simulations with a pair potential. Thus, one may resort, e.g., to effective potentials deduced from average atom models [32,33]. The wave numbers required for an appropriate extrapolation, however, will depend on the applicability of the GH and VE model under WDM conditions. Further, treating electrons dynamically [31] has an effect on the DSF. Provided the very narrow acoustic and diffusive peaks in the ion-ion DSF at small wave numbers can be resolved in future experiments, which requires meV resolution, it could become possible to accurately determine transport quantities such as the viscosity from experimental data [24].

ACKNOWLEDGMENTS

The author would like to thank Zoltan Donkó, Torben Ott, and Luciano Silvestri for providing data from their works, Michael Bonitz for helpful discussions, and the referees for constructive feedback and suggestions.

[1] *Frontiers and Challenges in Warm Dense Matter*, edited by F. Graziani, M. P. Desjarlais, R. Redmer, and S. B. Trickey (Springer International, Cham, 2014).

[2] J. Clérouin, P. Arnault, C. Ticknor, J. D. Kress, and L. A. Collins, Unified Concept of Effective One Component Plasma for Hot Dense Plasmas, Phys. Rev. Lett. **116**, 115003 (2016).

[3] J. J. Fortney and N. Nettelmann, The interior structure, composition, and evolution of giant planets, Space Sci. Rev. **152**, 423 (2010).

[4] M. D. Knudson, M. P. Desjarlais, R. W. Lemke, T. R. Mattsson, M. French, N. Nettelmann, and R. Redmer, Probing the Interiors of the Ice Giants: Shock Compression of Water to 700 GPa and 3.8 g/cm^3, Phys. Rev. Lett. **108**, 091102 (2012).

[5] F. Soubiran, B. Militzer, K. P. Driver, and S. Zhang, Properties of hydrogen, helium, and silicon dioxide mixtures in giant planet interiors, Phys. Plasmas **24**, 041401 (2017).

[6] J. Daligault and S. Gupta, Electron–ion scattering in dense multi-component plasmas: Application to the outer crust of an accreting neutron star, Astrophys. J. **703**, 994 (2009).

[7] M. E. Caplan, Structure of multicomponent Coulomb crystals, Phys. Rev. E **101**, 023201 (2020).

[8] O. A. Hurricane, D. A. Callahan, D. T. Casey, P. M. Celliers, C. Cerjan, E. L. Dewald, T. R. Dittrich, T. Döppner, D. E. Hinkel, L. F. Berzak Hopkins, J. L. Kline, S. LePape, T. Ma, A. G. MacPhee, J. L. Milovich, A. Pak, H.-S. Park, P. K. Patel, B. A. Remington, J. D. Salmonson, P. T. Springer, and R. Tommasini, Fuel gain exceeding unity in an inertially confined fusion implosion, Nature (London) **506**, 343 (2014).

[9] R. S. Craxton, K. S. Anderson, T. R. Boehly, V. N. Goncharov, D. R. Harding, J. P. Knauer, R. L. McCrory, P. W. McKenty, D. D. Meyerhofer, J. F. Myatt, A. J. Schmitt, J. D. Sethian, R. W. Short, S. Skupsky, W. Theobald, W. L. Kruer, K. Tanaka, R. Betti, T. J. B. Collins, J. A. Delettrez, S. X. Hu, J. A. Marozas, A. V. Maximov, D. T. Michel, P. B. Radha, S. P. Regan, T. C. Sangster, W. Seka, A. A. Solodov, J. M. Soures, C. Stoeckl, and J. D. Zuegel, Direct-drive inertial confinement fusion: A review, Phys. Plasmas **22**, 110501 (2015).

[10] R. Betti and O. A. Hurricane, Inertial-confinement fusion with lasers, Nat. Phys. **12**, 435 (2016).

[11] K. Falk, Experimental methods for warm dense matter research, High Power Laser Sci. **6**, E59 (2018).

[12] H. Sinn, F. Sette, U. Bergmann, C. Halcoussis, M. Krisch, R. Verbeni, and E. Burkel, Coherent Dynamic Structure Factor of Liquid Lithium by Inelastic X-ray Scattering, Phys. Rev. Lett. **78**, 1715 (1997).

[13] S. H. Glenzer and R. Redmer, X-ray Thomson scattering in high energy density plasmas, Rev. Mod. Phys. **81**, 1625 (2009).

[14] D. Kraus, B. Bachmann, B. Barbrel, R. W. Falcone, L. B. Fletcher, S. Frydrych, E. J. Gamboa, M. Gauthier, D. O. Gericke, S. H. Glenzer, S. Göde, E. Granados, N. J. Hartley, J. Helfrich, H. J. Lee, B. Nagler, A. Ravasio, W. Schumaker, J. Vorberger, and T. Döppner, Characterizing the ionization potential depression in dense carbon plasmas with high-precision spectrally resolved x-ray scattering, Plasma Phys. Control. Fusion **61**, 014015 (2018).

[15] K. Falk, M. Holec, C. J. Fontes, C. L. Fryer, C. W. Greeff, H. M. Johns, D. S. Montgomery, D. W. Schmidt, and M. Šmíd, Measurement of Preheat due to Nonlocal Electron Transport in Warm Dense Matter, Phys. Rev. Lett. **120**, 025002 (2018).

[16] J. Valenzuela, C. Krauland, D. Mariscal, I. Krasheninnikov, C. Niemann, T. Ma, P. Mabey, G. Gregori, P. Wiewior, A. Covington *et al.*, Measurement of temperature and density using non-collective x-ray Thomson scattering in pulsed power produced warm dense plasmas, Sci. Rep. **8**, 8432 (2018).

[17] Y. Kuwayama, G. Morard, Y. Nakajima, K. Hirose, A. Q. R. Baron, S. I. Kawaguchi, T. Tsuchiya, D. Ishikawa, N. Hirao, and Y. Ohishi, Equation of State of Liquid Iron under Extreme Conditions, Phys. Rev. Lett. **124**, 165701 (2020).

[18] T. Dornheim, S. Groth, J. Vorberger, and M. Bonitz, *Ab initio* Path Integral Monte Carlo Results for the Dynamic Structure Factor of Correlated Electrons: From the Electron Liquid to Warm Dense Matter, Phys. Rev. Lett. **121**, 255001 (2018).

[19] S. H. Glenzer, O. L. Landen, P. Neumayer, R. W. Lee, K. Widmann, S. W. Pollaine, R. J. Wallace, G. Gregori, A. Höll, T. Bornath, R. Thiele, V. Schwarz, W.-D. Kraeft, and R. Redmer, Observations of Plasmons in Warm Dense Matter, Phys. Rev. Lett. **98**, 065002 (2007).

[20] L. B. Fletcher, H. J. Lee, T. Döppner, E. Galtier, B. Nagler, P. Heimann, C. Fortmann, S. LePape, T. Ma, M. Millot, A. Pak, D. Turnbull, D. A. Chapman, D. O. Gericke, J. Vorberger, T. White, G. Gregori, M. Wei, B. Barbrel, R. W. Falcone, C.-C. Kao, H. Nuhn, J. Welch, U. Zastrau, P. Neumayer, J. B. Hastings, and S. H. Glenzer, Ultrabright x-ray laser scattering for dynamic warm dense matter physics, Nat. Photonics **9**, 274 (2015).

[21] P. Sperling, E. J. Gamboa, H. J. Lee, H. K. Chung, E. Galtier, Y. Omarbakiyeva, H. Reinholz, G. Röpke, U. Zastrau, J. Hastings, L. B. Fletcher, and S. H. Glenzer, Free-Electron X-ray Laser Measurements of Collisional-Damped Plasmons in Isochorically Heated Warm Dense Matter, Phys. Rev. Lett. **115**, 115001 (2015).

[22] S. H. Glenzer, L. B. Fletcher, E. Galtier, B. Nagler, R. Alonso-Mori, B. Barbrel, S. B. Brown, D. A. Chapman, Z. Chen, C. B. Curry, F. Fiuza, E. Gamboa, M. Gauthier, D. O. Gericke, A. Gleason, S. Goede, E. Granados, P. Heimann, J. Kim, D. Kraus, M. J. MacDonald, A. J. Mackinnon, R. Mishra, A. Ravasio, C. Roedel, P. Sperling, W. Schumaker, Y. Y. Tsui, J. Vorberger, U. Zastrau, A. Fry, W. E. White, J. B. Hasting, and H. J. Lee, Matter under extreme conditions experiments at the Linac Coherent Light Source, J. Phys. B: At. Mol. Opt. Phys. **49**, 092001 (2016).

[23] T. Tschentscher, C. Bressler, J. Grünert, A. Madsen, A. Mancuso, M. Meyer, A. Scherz, H. Sinn, and U. Zastrau, Photon beam transport and scientific instruments at the European XFEL, Appl. Sci. **7**, 592 (2017).

[24] E. E. McBride, T. G. White, A. Descamps, L. B. Fletcher, K. Appel, F. P. Condamine, C. B. Curry, F. Dallari, S. Funk, E. Galtier, M. Gauthier, S. Goede, J. B. Kim, H. J. Lee, B. K. Ofori-Okai, M. Oliver, A. Rigby, C. Schoenwaelder, P. Sun, T. Tschentscher, B. B. L. Witte, U. Zastrau, G. Gregori, B. Nagler, J. Hastings, S. H. Glenzer, and G. Monaco, Setup for mev-resolution inelastic x-ray scattering measurements and x-ray diffraction at the matter in extreme conditions endstation at the Linac Coherent Light Source, Rev. Sci. Instrum. **89**, 10F104 (2018).

[25] J. Chihara, Interaction of photons with plasmas and liquid metals - photoabsorption and scattering, J. Phys.: Condens. Matter **12**, 231 (1999).

[26] M. Bonitz, T. Dornheim, Z. A. Moldabekov, S. Zhang, P. Hamann, H. Kählert, A. Filinov, K. Ramakrishna, and J. Vorberger, *Ab initio* simulation of warm dense matter, Phys. Plasmas **27**, 042710 (2020).

[27] T. G. White, S. Richardson, B. J. B. Crowley, L. K. Pattison, J. W. O. Harris, and G. Gregori, Orbital-Free Density-Functional Theory Simulations of the Dynamic Structure Factor of Warm Dense Aluminum, Phys. Rev. Lett. **111**, 175002 (2013).

[28] H. R. Rüter and R. Redmer, *Ab Initio* Simulations for the Ion-Ion Structure Factor of Warm Dense Aluminum, Phys. Rev. Lett. **112**, 145007 (2014).

[29] P. Mabey, S. Richardson, T. White, L. Fletcher, S. Glenzer, N. Hartley, J. Vorberger, D. Gericke, and G. Gregori, A strong diffusive ion mode in dense ionized matter predicted by Langevin dynamics, Nat. Commun. **8**, 14125 (2017).

[30] B. B. L. Witte, M. Shihab, S. H. Glenzer, and R. Redmer, *Ab initio* simulations of the dynamic ion structure factor of warm dense lithium, Phys. Rev. B **95**, 144105 (2017).

[31] B. Larder, D. O. Gericke, S. Richardson, P. Mabey, T. G. White, and G. Gregori, Fast nonadiabatic dynamics of many-body quantum systems, Sci. Adv. **5**, eaaw1634 (2019).

[32] N. M. Gill, R. A. Heinonen, C. E. Starrett, and D. Saumon, Ion-ion dynamic structure factor of warm dense mixtures, Phys. Rev. E **91**, 063109 (2015).

[33] L. Harbour, G. D. Förster, M. W. C. Dharma-wardana, and L. J. Lewis, Ion-ion dynamic structure factor, acoustic modes, and equation of state of two-temperature warm dense aluminum, Phys. Rev. E **97**, 043210 (2018).

[34] Z. A. Moldabekov, H. Kählert, T. Dornheim, S. Groth, M. Bonitz, and T. S. Ramazanov, Dynamical structure factor of strongly coupled ions in a dense quantum plasma, Phys. Rev. E **99**, 053203 (2019).

[35] J. P. Mithen, J. Daligault, and G. Gregori, Extent of validity of the hydrodynamic description of ions in dense plasmas, Phys. Rev. E **83**, 015401(R) (2011).

[36] J. P. Mithen, J. Daligault, B. J. B. Crowley, and G. Gregori, Density fluctuations in the Yukawa one-component plasma: An accurate model for the dynamical structure factor, Phys. Rev. E **84**, 046401 (2011).

[37] J. Mithen, Molecular dynamics simulations of the equilibrium dynamics of non-ideal plasmas, Ph.D. thesis, Oxford University, 2012.

[38] J. Vorberger, Z. Donkó, I. M. Tkachenko, and D. O. Gericke, Dynamic Ion Structure Factor of Warm Dense Matter, Phys. Rev. Lett. **109**, 225001 (2012).

[39] J. Hong and C. Kim, Dynamic structure of strongly coupled one-component plasmas, Phys. Rev. A **43**, 1965 (1991).

[40] C. Fortmann, A. Wierling, and G. Röpke, Influence of local-field corrections on Thomson scattering in collision-dominated two-component plasmas, Phys. Rev. E **81**, 026405 (2010).

[41] Y. V. Arkhipov, A. Askaruly, D. Ballester, A. E. Davletov, I. M. Tkachenko, and G. Zwicknagel, Dynamic properties of one-component strongly coupled plasmas: The sum-rule approach, Phys. Rev. E **81**, 026402 (2010).

[42] Y. Choi, G. Dharuman, and M. S. Murillo, High-frequency response of classical strongly coupled plasmas, Phys. Rev. E **100**, 013206 (2019).

[43] Y. V. Arkhipov, A. Askaruly, A. E. Davletov, D. Y. Dubovtsev, Z. Donkó, P. Hartmann, I. Korolov, L. Conde, and I. M. Tkachenko, Direct Determination of Dynamic Properties of Coulomb and Yukawa Classical One-Component Plasmas, Phys. Rev. Lett. **119**, 045001 (2017).

[44] U. Balucani and M. Zoppi, *Dynamics of the Liquid State* (Clarendon Press, Oxford, 1995).

[45] J. P. Boon and S. Yip, *Molecular Hydrodynamics* (Dover publications, New York, 1991).

[46] J. P. Hansen and I. R. McDonald, *Theory of Simple Liquids* (Elsevier Academic Press, London, 2006).

[47] M. S. Murillo, Viscosity estimates of liquid metals and warm dense matter using the Yukawa reference system, High Energ. Dens. Phys. **4**, 49 (2008).

[48] K. Wünsch, J. Vorberger, and D. O. Gericke, Ion structure in warm dense matter: Benchmarking solutions of hypernetted-chain equations by first-principle simulations, Phys. Rev. E **79**, 010201(R) (2009).

[49] S. Hamaguchi, R. T. Farouki, and D. H. E. Dubin, Triple point of Yukawa systems, Phys. Rev. E **56**, 4671 (1997).

[50] S. A. Khrapak and H. M. Thomas, Fluid approach to evaluate sound velocity in Yukawa systems and complex plasmas, Phys. Rev. E **91**, 033110 (2015).

[51] S. A. Khrapak, Thermodynamics of Yukawa systems and sound velocity in dusty plasmas, Plasma Phys. Control. Fusion **58**, 014022 (2015).

[52] Z. Donkó and P. Hartmann, Thermal conductivity of strongly coupled Yukawa liquids, Phys. Rev. E **69**, 016405 (2004).

[53] Z. Donkó and P. Hartmann, Shear viscosity of strongly coupled Yukawa liquids, Phys. Rev. E **78**, 026408 (2008).

[54] J. Daligault, K. O. Rasmussen, and S. D. Baalrud, Determination of the shear viscosity of the one-component plasma, Phys. Rev. E **90**, 033105 (2014).

[55] T. Ott, M. Bonitz, and Z. Donkó, Effect of correlations on heat transport in a magnetized strongly coupled plasma, Phys. Rev. E **92**, 063105 (2015).

[56] T. Ott, M. Bonitz, P. Hartmann, and Z. Donkó, Spontaneous generation of temperature anisotropy in a strongly coupled magnetized plasma, Phys. Rev. E **95**, 013209 (2017).

[57] M. Lyon and S. L. Rolston, Ultracold neutral plasmas, Rep. Prog. Phys. **80**, 017001 (2017).

[58] M. Bonitz, N. Horing, and P. Ludwig (eds.) *Introduction to Complex Plasmas* (Springer, Berlin, 2010).

[59] A. Ivlev, H. Löwen, G. Morfill, and C. P. Royall, *Complex Plasmas and Colloidal Dispersions: Particle-resolved Studies of Classical Liquids and Solids* (World Scientific, Singapore, 2012).

[60] U. Bafile, E. Guarini, and F. Barocchi, Collective acoustic modes as renormalized damped oscillators: Unified description of neutron and x-ray scattering data from classical fluids, Phys. Rev. E **73**, 061203 (2006).

[61] E. Guarini, S. Bellissima, U. Bafile, E. Farhi, A. De Francesco, F. Formisano, and F. Barocchi, Density of states from mode expansion of the self-dynamic structure factor of a liquid metal, Phys. Rev. E **95**, 012141 (2017).

[62] L. G. Silvestri, G. J. Kalman, Z. Donkó, P. Hartmann, M. Rosenberg, K. I. Golden, and S. Kyrkos, Sound speed in Yukawa one-component plasmas across coupling regimes, Phys. Rev. E **100**, 063206 (2019).

[63] H. Kählert, Dynamic structure factor of strongly coupled Yukawa plasmas with dissipation, Phys. Plasmas **26**, 063703 (2019).

[64] F. Nardin, G. Jacucci, and M. W. C. Dharma-wardana, Dynamic ion-ion structure factor of strongly coupled hydrogen plasmas at arbitrary degeneracies, Phys. Rev. A **37**, 1025 (1988).

[65] F. Barocchi, E. Guarini, and U. Bafile, Exponential series expansion for correlation functions of many-body systems, Phys. Rev. E **90**, 032106 (2014).

[66] I. Korolov, G. J. Kalman, L. Silvestri, and Z. Donkó, The dynamical structure function of the one-component plasma revisited, Contrib. Plasma Phys. **55**, 421 (2015).

[67] S. Khrapak, Practical formula for the shear viscosity of Yukawa fluids, AIP Adv. **8**, 105226 (2018).

[68] G. Salin and J.-M. Caillol, Transport Coefficients of the Yukawa One-Component Plasma, Phys. Rev. Lett. **88**, 065002 (2002).

[69] H. Kählert, G. J. Kalman, and M. Bonitz, Linear fluid theory for weakly inhomogeneous plasmas with strong correlations, Contrib. Plasma Phys. **55**, 352 (2015).

[70] S. A. Khrapak, Relations between the longitudinal and transverse sound velocities in strongly coupled Yukawa fluids, Phys. Plasmas **23**, 024504 (2016).

[71] S. Khrapak, B. Klumov, and L. Couëdel, Collective modes in simple melts: Transition from soft spheres to the hard sphere limit, Sci. Rep. **7**, 7985 (2017).

[72] J. Goree, Z. Donkó, and P. Hartmann, Cutoff wave number for shear waves and Maxwell relaxation time in Yukawa liquids, Phys. Rev. E **85**, 066401 (2012).